Lipid model membrane systems as a tool for unraveling the underlying factors for skin barrier dysfunction

Uche, L.E.

3

High concentration of the ester-linked -hydroxy ceramide increases the permeability in skin lipid model membranes

Authors and affiliations:
Lorretta.E. Uche[1], Gerrit.S. Gooris[1], Joke.A. Bouwstra[1] and Charlotte.M. Beddoes[1]

[1]Division of Drug Delivery Technology, Cluster BioTherapeutics, Leiden Academic Centre for Drug Research, Leiden University, Netherlands

Adapted from: Biochimica et Biophysica Acta (BBA) - Biomembranes, 2021. **1863**(1): p. 183487-183497.

ABSTRACT

The ester-linked ω-hydroxy acyl chain linked to a sphingosine base referred to as CER EOS is essential for the skin barrier lipid organization. While the majority of the skin lipids form a dense, crystalline structure, associated with low permeability, the unsaturated moiety of CER EOS, (either the linoleate or the oleate chain) exists in a liquid phase at the skin's physiological temperature. Thus, the relationship between CER EOS and barrier function is not entirely comprehended. We studied the permeability and lipid organization in skin lipid models, gradually increasing in CER EOS concentration, mixed with non-hydroxy sphingosine-based ceramide (CER NS) in an equimolar ratio of CERs, cholesterol, and free fatty acids (FFAs) mimicking the ratio in the native skin. A significant increase in the orthorhombic-hexagonal phase transition temperature was recorded when CER EOS concentration was raised to 70 mol% of the total CER content and higher, rendering a higher fraction of lipids in the orthorhombic phase at the expense of the hexagonal phase at physiological temperature. The model's permeability did not differ when CER EOS concentration ranged between 10 to 30% but increased significantly at 70% and higher. Using CER EOS with a perdeuterated oleate chain, it was shown that the fraction of lipids in a liquid phase increased with CER EOS concentration, while the neighboring CERs and FFAs remained in a crystalline state. The increased fraction of the liquid phase therefore, had a stronger effect on permeability than the increased fraction of lipids forming an orthorhombic phase.

Keywords:
Intercellular lipid; Stratum corneum; Infrared spectroscopy; X-ray diffraction; Long periodicity phase; Sphingolipids.

INTRODUCTION

The skin protects the body from the invasion of pathogens and other harmful substances in the external environment, as well as preventing desiccation from within. This skin's barrier function is ascribed to its thin outermost layer known as the stratum corneum (SC) [1-3]. The SC comprises of keratin-filled, flattened dead cells referred to as corneocytes, embedded in a lipid matrix. The corneocytes show a reduced permeability by the presence of a densely cross-linked protein envelope thereby redirecting the permeation of substances along the intercellular lipid matrix [4-6]. Consequently, the composition and organization of the SC lipids are essential to the barrier function.

The SC lipids are arranged into intercellular lamellae aligned approximately parallel to the cell surface [7]. Two distinct lamellar phases, the long periodicity phase (LPP) and the short periodicity phase (SPP) are detected by X-ray diffraction studies [8, 9]. The LPP is exclusively present in the SC and is considered to be important for the skin barrier function [10, 11]. X-ray and neutron diffraction revealed that the LPP is a trilayer structure [12, 13]. Perpendicular to the basal layer of the lamellae, the lipids adopt predominantly the dense orthorhombic lateral packing. This packing plays a role in the low permeability of the skin barrier [14].

The SC intercellular lipid domains are primarily composed of approximately an equimolar ratio of cholesterol (CHOL), free fatty acids (FFAs), and ceramides (CERs) [15, 16]. The FFAs are predominantly saturated and display a chain length distribution between 12 and 30 carbon atoms [17, 18]. CERs are a structurally heterogeneous group of sphingolipids, comprising of a sphingoid base linked to an acyl chain via an amide bond. Currently, at least 18 CER subclasses have been identified in human SC [19-23]. Four of the subclasses often referred to as acylCERs, constitute of an ultra-long ω-hydroxy acyl chain, which contains up to 30-34 carbon atoms, ester-linked to an unsaturated fatty acid (usually linoleic acid) and amide-linked to one of the various sphingoid bases. These acyl CERs are only present in the SC and their concentration is reduced in skin diseases such as atopic dermatitis, psoriasis, Netherton syndrome, and autosomal recessive congenital ichthyosis, but also in dry skin [24-30]. Consequently, their role in barrier function has attracted attention [10, 31, 32]. The relative abundance of the acylCERs is ~8-13 mol% of the total CERs in the human SC [33, 34]. The most abundant acylCER is the subclass with a sphingosine (S) base referred to as CER EOS [33]. Using lipid models prepared with both isolated [35-38] and synthetic CER mixtures [31, 39], it was shown that CER EOS is efficient in enhancing the

formation of the LPP. Previous FTIR and NMR studies reported that the linoleate moiety of CER EOS linoleate (CER EOS-L) (Fig. 1A) exists in a disordered fluid phase in a crystalline environment of the SC model [40, 41]. In the present study, a similar behavior was reported for the oleate moiety of CER EOS oleate (CER EOS-O) (Fig. 1B), which is in agreement with another recent study using FTIR, Raman spectroscopy, and NMR techniques [42]. Another NMR study showed that concerning the linoleate chain, the fluidity is primarily located in the middle and end segment of the chain [40]. With regards to the effect of CER EOS on barrier function, SC model membranes prepared with synthetic CERs, that mimicked the composition in pig SC, showed a two-fold increase in permeability of ethyl para-aminobenzoic acid when CER EOS was excluded from the lipid composition [10]. In another study, incorporation of 10% CER EOS resulted in an increase in permeability of theophylline and indomethacin across a simple SC model compared to that in the absence of CER EOS, but the permeability reduced as CER EOS concentration was increased up to 30% [31]. Opalka et al. further reported that the permeability of a complex lipid model was not improved when the content of either an individual acylCER or an acylCER mixture was increased above the physiological concentration to 30% [43]. However, the barrier function in relation to the fraction of lipids forming co-existing crystalline and liquid phases was not studied, neither was the effect of concentrations of CER EOS beyond 30% investigated.

Therefore, in the present study, we aimed to determine the effect of increasing the concentration of CER EOS on the lipid phase behavior and barrier function. To achieve our purpose, SC models were used with a composition that systematically increased in CER EOS concentration between 10-90% mol of the total CER content. We incorporated CER NS in the models since SC

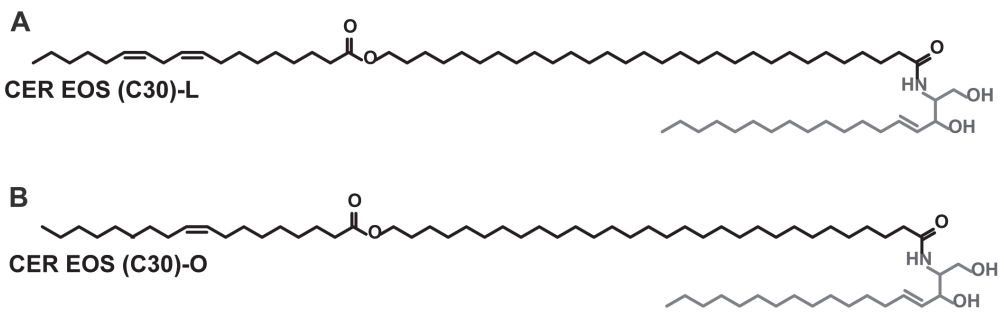

Fig. 1: Molecular structure of the acylCERs used in the study.

The CERs consist of an unsaturated fatty acid esterified to an ω-hydroxy fatty acid acyl chain (black), which is linked to a sphingoid base (grey) via an amide bond. The unsaturated fatty acid is either A) linoleic acid (CER EOS (C30)-L) or B) oleic acid (CER EOS (C30)-O).

models prepared with CER NS easily formed the LPP [44-46]. Furthermore, this composition allowed us to use deuterated CERs, which provide more detailed insight into the lipid phase behavior. Small-angle X-ray diffraction (SAXD) and Fourier transform infrared spectroscopy (FTIR) were used to study the lipid arrangement and phase behavior of the models. The barrier function of the models was assessed by carrying out permeation studies and transepidermal water loss (TEWL) measurements.

EXPERIMENTAL SECTION

Materials

The synthetic CERs used in the study: i) N-(tetracosanoyl)-sphingosine (CER NS C24), ii) CER NS C24 with a deuterated fatty acid chain denoted as D-NS, iii) N-(30-Linoleoyloxy-triacontanoyl)-sphingosine (CER EOS (C30)-L), and iv) CER EOS (C30)-O with deuterated oleate chain denoted as D-EOS, were generously donated by Evonik (Essen, Germany). The CERs had a purity of ≥ 90% (as determined by mass spectrometry). Using mass spectrometry method for CER analysis [47], the CERs had a purity of ≥ 98%. CHOL, ethyl-p-aminobenzoate (E-PABA), acetate buffer salts, and the FFAs: palmitic acid (C16), stearic acid (C18), arachidic acid (C20), behenic acid (C22), and lignoceric acid (C24), were purchased from Sigma-Aldrich Chemie GmbH (Schnelldorf, Germany). The perdeuterated FFAs (DFFAs) with chain lengths of C18 and C20 were obtained from Cambridge Isotope Laboratories (Andover, Massachusetts). The DFFAs with chain lengths of C16 and C22 were purchased from Larodan (Malmö, Sweden). The DFFA with a chain length of C24 was obtained from Arc Laboratories B.V. (Apeldoorn, The Netherlands). All organic solvents were of analytical grade. The water was of Millipore quality, obtained through a Milli-Q Integral water purification system with a resistivity of 18 MΩ cm at 25°C (Millipore, Bedford, MA). Nucleopore polycarbonate filter disks (pore size 0.05 µm) were purchased from Whatman (Kent, UK).

Composition of the model lipid mixtures

SC lipid models were prepared as equimolar mixtures of CER, CHOL, and FFAs. The FFA component comprised of C16, C18, C20, C22, and C24 at relative molar percentages of 1.8, 4.0, 7.6, 47.8, and 38.8 respectively, a composition adapted from the FFA composition in the native SC [17]. The CER fraction of the models differed by the CER EOS concentration (10/30/50/70/90 mol%) and was

counterbalanced with CER NS. The resulting lipid models are named EOS-10, EOS-30, EOS-50, EOS-70, and EOS-90. Secondly, similar models were prepared but with the FFAs replaced by their deuterated counterparts (CER EOS/CER NS/CHOL/DFFAs) denoted by -DFFA as a suffix to the model name. In the third set of models, the fatty acid acyl chain of CER NS was replaced with the deuterated chain (CER EOS/CER D-NS/CHOL/FFAs), resulting in the models identified by the suffix -D-NS. Finally, since CER EOS with deuterated linoleate chain, is not available, the oleate counterpart was used in the preparation of the fourth set of models (CER D-EOS/CER NS/CHOL/FFAs). Therein, the oleate moiety of CER EOS oleate was substituted with the deuterated counterpart and the resulting models are denoted by D- as a prefix to the model name. CER EOS linoleate and oleate are structural analogues (Fig. 1) and have a similar influence on lipid phase behavior in SC models both resulting in similar phase transition temperatures and leading to the formation of LPP in SC models [37, 48]. The composition of the models are shown in table 1.

Table 1: Composition of the various models used in this study. CER:CHOL:FFA mixture is prepared as equimolar. For clarification, the CER EOS concentration in this study refers to the percentage of CER EOS relative to the CER fraction, not the total lipid content.

Lipid model name	Composition and molar ratio (1:1:1)
EOS-10	[EOS(C30)-L 10% + NS(C24) 90%]: CHOL: FFAs
EOS-30	[EOS(C30)-L 30% + NS(C24) 70%]: CHOL: FFAs
EOS-50	[EOS(C30)-L 50% + NS(C24) 50%]: CHOL: FFAs
EOS-70	[EOS(C30)-L 70% + NS(C24) 30%]: CHOL: FFAs
EOS-90	[EOS(C30)-L 90% + NS(C24) 60%]: CHOL: FFAs
EOS-10-DFFA	[EOS(C30)-L 10% + NS(C24) 90%]: CHOL: DFFAs
EOS-30-DFFA	[EOS(C30)-L 30% + NS(C24) 70%]: CHOL: DFFAs
EOS-50-DFFA	[EOS(C30)-L 50% + NS(C24) 50%]: CHOL: DFFAs
EOS-70-DFFA	[EOS(C30)-L 70% + NS(C24) 30%]: CHOL: DFFAs
EOS-90-DFFA	[EOS(C30)-L 90% + NS(C24) 60%]: CHOL: DFFAs
EOS-10-D-NS	[EOS(C30)-L 10% + D-NS(C24) 90%]: CHOL: FFAs
EOS-30-D-NS	[EOS(C30)-L 30% + D-NS(C24) 70%]: CHOL: FFAs
EOS-70-D-NS	[EOS(C30)-L 70% + D-NS(C24) 30%]: CHOL: FFAs
D-EOS-10	[D-EOS(C30)-O 10% + NS(C24) 90%]: CHOL: FFAs
D-EOS-30	[D-EOS(C30)-O 30% + NS(C24) 70%]: CHOL: FFAs
D-EOS-70	[D-EOS(C30)-O 70% + NS(C24) 30%]: CHOL: FFAs

Preparation of samples for permeability studies, X-ray diffraction, and FTIR spectroscopy

For the permeability and X-ray diffraction studies, 0.9mg of the appropriate lipid composition was dissolved in 200 µl hexane:ethanol (2:1) solution, to a final concentration of 4.5 mg/ml. For FTIR spectroscopy, 1.5 mg of the applicable lipid composition was dissolved in chloroform:methanol (2:1) to a concentration of 5 mg/ml. Using a Linomat IV device (Camag, Muttenz, Switzerland) the solution was sprayed on a suitable substrate (nucleopore polycarbonate filter disk with 0.05 µm pore size for the permeability and X-ray studies, and AgBr window for FTIR spectroscopy). It was necessary to use hexane:ethanol as solvent for spraying on the polycarbonate membrane since this membrane is not resistant to chloroform [49]. However, this did not cause any difference in phase behaviour. Spraying was performed at the rate of 14 µl/sec, over an area of 10 x 10 mm^2, under a gentle stream of nitrogen. An approximate distance of 1 mm was maintained between the nozzle and the spraying surface. The samples were equilibrated at 85 °C for 30 min, which was sufficient to ensure that the lipid mixtures had fully melted, and then gradually cooled to room temperature. Finally, the samples for X-ray studies were hydrated over 27% NaBr in milli-Q water (water vapour) for at least 15 h. While FTIR samples were hydrated in deuterated acetate buffer (pH 5.0) and incubated at 37 °C for at least 15 h to ensure that the samples were fully hydrated. The membranes used in permeability studies were thus hydrated with phosphate-buffered saline inside the flow-through diffusion cell to mimic the in-vivo situation as much as possible [49].

Permeability studies

Permegear in-line diffusion cells (Bethlehem PA, USA) with a diffusion area of 0.28 cm^2 were used for the *in-vitro* permeation studies. The model membranes were mounted in the diffusion cells and hydrated for an hour with the acceptor phase consisting of phosphate-buffered saline (PBS 0.1 M solution: NaCl, Na_2HPO_4, KH_2PO_4, and KCl in milli-Q water with a concentration of 8.13, 1.14, 0.20, and 0.19 g/l respectively) at pH 7.4 prior to the experiment. Before use, the PBS was filtered and degassed. The donor compartment consisted of 1400 µl of a saturated E-PABA (0.65mg/ml) in acetate buffer solution (pH 5) and was sealed with an adhesive tape to prevent solvent evaporation. The acceptor phase was constantly stirred and perfused at a flow rate of 2 ml/h through an in-line degasser to remove air bubbles that may form during the experiment. The temperature of the membranes was maintained at 32 °C. The acceptor fluid was collected over 15 h at 1-hour intervals. At the end of the diffusion study, the volume per collected

fraction of PBS was determined by weight and the concentration of E-PABA was determined by ultra performance liquid chromatography (UPLC). The flux of E-PABA was calculated using Fick's first law of diffusion [50]. Permeation of multiple samples of each composition was analyzed, n > 4. The steady-state flux values were calculated using a time interval between the 5th and 15th hour.

UPLC analysis

UPLC was run with Acquity UPLC systems (Waters Co., Milford, MA, USA) for the analysis of E-PABA. The UPLC systems consisted of a quaternary solvent manager (a high-pressure pump), a tunable ultraviolet/visible absorbance detector, and a sample manager. The stationary phase consisted of a UPLC special analytical column packed with 1.7 µm, bridged, ethyl siloxane, hybrid particles. The column temperature was set at 40 °C. The mobile phase was composed of a mixture of 0.1% trifluoroacetic acid in acetonitrile: milli-Q water at 40:60 (v/v) ratio. The flow rate of the mobile phase was 1 ml/min. 10 µl of the sample was injected on the column. The detector wavelength was set at 286 nm. Data were collected and processed by MassLynx and TargetLynx software V4.1 SCN951 (Waters Co., Milford, USA).

The standard stock solution of E-PABA, 0.5 mg/ml was prepared in a 1:1 solution of methanol and milli-Q. Ten different concentrations were prepared by serial dilutions from the stock, with milli-Q water, to plot the standard curve. The linearity of the relationship was evaluated in a concentration range between 0.1 -10 µg/ml covering the range of concentrations obtained when analyzing the concentration of E-PABA permeating the model membranes. The calibration curves were obtained using least square linear regression fitting and the linearity was confirmed with the R^2 values. R^2 value very close to 1 indicates excellent linearity.

The UPLC method was previously validated for E-PABA analysis as per ICH (International conference on harmonization) guidelines concerning linearity, precision, limit of detection (LOD), and limit of quantification (LOQ) [46, 51, 52].

TEWL measurements

An AquaFlux (AF200, Biox Systems Ltd., London, UK) was used to measure the water loss from the lipid models. The measurement has been previously described elsewhere [50]. Briefly, the sprayed membranes were mounted in flow-through diffusion cells, which were subsequently filled with milli-Q water. The cells were left to hydrate for at least 30min before measuring. The TEWL device was then coupled vertically with the donor compartment of the diffusion

cell using a special measurement cap (Biox Systems Limited, UK) in order to seal the compartment and ensure vapour tight connectivity. The TEWL values for the models studied were recorded for 30 min. The final 10 min of the measurement was used to calculate the TEWL value, n = 7.

Data analysis for the permeability and TEWL measurements.

One-way ANOVA with Bonferroni's multiple comparison test was performed to analyze the permeability and TEWL data. Differences in mean are considered statistically significant when $P < 0.05$.

FTIR measurements

FTIR spectra were acquired on a Varian 670-IR spectrometer (Agilent Technologies, Inc., Santa Clara, CA) equipped with a broad-band mercury cadmium telluride detector, cooled by liquid nitrogen. The sample was kept under a continuous dry air purge, starting 30 min before data acquisition. The spectra were generated in the transmission mode by the coaddition of 256 interferograms, at a resolution of 1 cm^{-1}, collected over 4 min. To determine the phase transitions in relation to the temperature, the spectra were collected between 0 – 100 °C at a heating rate of 0.25 °C/ min, resulting in a 1 °C temperature rise per recorded spectrum. Samples were measured over a range of 600–4000 cm^{-1}. The spectra were deconvoluted using a half-width of 4 cm^{-1}, and an enhancement factor of 1.6. The software used was Agilent resolution pro (Agilent Technologies, Palo Alto CA, USA). The conformational ordering and phase transition of the lipid chains were obtained by examination of the protiated methylene symmetric stretching modes observed at ~ 2850 cm^{-1} and the deuterated symmetric stretching modes at ~ 2090 cm^{-1}, referred to as $\nu_s CH_2$ and $\nu_s CD_2$ modes respectively. The linear regression curve fitting method was used to determine the mid-transition temperature as described previously [53]. The CH_2 scissoring mode (δCH_2), 1462–1473 cm^{-1}, and CD_2 scissoring mode (δCD_2), 1085–1095 cm^{-1} were analyzed to evaluate the lateral packing and mixing properties of the lipid chains respectively. Multiple samples of each composition were measured, n > 2.

SAXD studies

To determine the long-range ordering, SAXD experiments were conducted at the European Synchrotron Radiation Facility (ESRF, Grenoble) at station BM26B. The X-ray wavelength (λ) was 0.1033 nm and the sample-to-detector distance was 2.1 m. Diffraction patterns were recorded using a Pilatus 1M detector. The spatial calibration of the detector was performed using silver behenate. Samples were

measured for 90 s. The scattering intensity (*I*) was measured as a function of the scattering vector (*q)* which is proportional to the scattering angle (θ) according to the equation, defined as $q = \frac{4\pi \sin\theta}{\lambda}$. From the positions of a series of equidistant peaks (q_h), the periodicity of a lamellar phase was calculated using the equation $d = \frac{2h\pi}{q_h}$ in which *h* is the order of the diffraction peak. Samples were prepared and measured in triplicate. The peak intensities attributed to the LPP were determined from the SAXD patterns, fitted with a Voigt function in the software Fityk [54].

RESULTS

A high concentration of CER EOS increases the permeability of the SC model membranes

To evaluate the effect of CER EOS concentration on the permeability of the model membranes, we compared their permeability to E-PABA. The average fluxes of E-PABA across the models with a gradual increase in CER EOS concentration are displayed in Fig. 2A. The E-PABA average steady-state flux values are plotted in Fig. 2B. Increasing the CER EOS concentration from 10 to 30% of the total CER fraction in the model membrane resulted in no significant difference in permeability (7.8 ± 2.9 to 8.2 ± 4.8 μg/cm^2/h). On further increase in CER EOS concentration to 50, 70, and 90%, the permeability increased (14.5 ± 8.6, 22.2 ± 5.0 and 25.2 ± 3.3 μg/cm^2/h respectively), with EOS-70 and EOS-90 being significantly more permeable than EOS-10 and EOS-30.

Water transport was also monitored by performing TEWL measurements. The water loss across EOS-90 and EOS-70 was 3.5 ± 0.2 and 2.9 ± 0.5 μg/m^2/h respectively, both significantly higher than that across EOS-30 (1.8 ± 0.2 μg/m^2/h). See Fig. 2C.

The phase transition temperature and packing density of the lipid chains are higher with increasing CER EOS concentration

The packing density of the lipids is important for understanding the changes in permeability at increasing CER EOS content. In the FTIR spectrum, $\nu_s CH_2$ and δCH_2 frequencies provide information about lipid chain conformational ordering and packing density [55-57]. The thermotropic response of the $\nu_s CH_2$ modes of EOS-10 and EOS-90 are plotted in Fig. 3A. The initial wavenumber of the fully protiated models appeared below 2850 cm^{-1} indicating highly ordered hydrocarbon chains [56, 58]. EOS-90 $\nu_s CH_2$ wavenumber was higher than that of EOS-10 suggesting lower conformational ordering of the lipid chains, but the

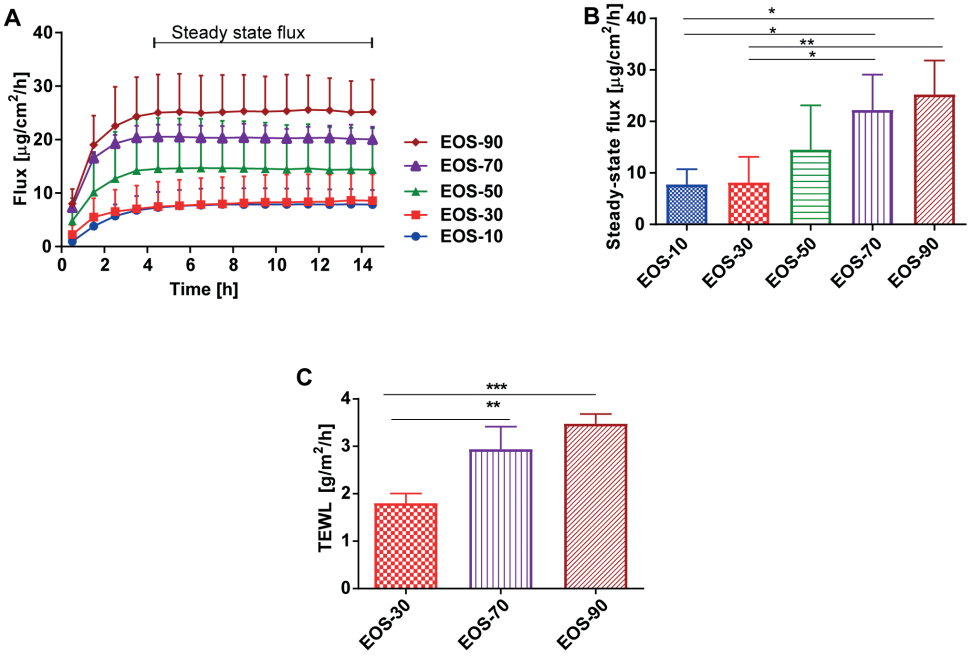

Fig. 2: Permeability of the model membranes.

A) Average flux of E-PABA across the model membranes over 15 h. B) The average steady-state flux of E-PABA across the model membranes (5-15 h). Data presented as the mean ± SD, n ≥ 4. E-PABA steady-state flux was significantly higher in EOS-70 and EOS-90. C) TEWL across the model membranes, EOS-70 and EOS-90 showing significantly higher permeability compared to EOS-30, n ≥ 3, [*P < 0.05, **P < 0.01, ***P < 0.001].

difference was not significant. The increase in temperature between 20 and 40 °C resulted in an approximate 1 cm^{-1} rise in the wavenumber, representing the orthorhombic-hexagonal phase transition. Further increase in temperature resulted in a larger wavenumber shift of 3-4 cm^{-1} between 60 and 80 °C. This indicates the transition from a hexagonal to the disordered liquid phase [59, 60]. The midpoint temperatures of the orthorhombic-hexagonal phase transition ($T_{M,OR-HEX}$) in the various fully protiated models are presented in Fig. 3B. The $T_{M,OR-HEX}$ increased gradually with increasing CER EOS concentration.

Concerning the lateral packing of the lipid chains, the δCH_2 mode was split into two peaks, centered at ~ 1462 cm^{-1} and 1473 cm^{-1} signifying an orthorhombic packing [59, 61]. This doublet is a direct result of short-range coupling between adjacent hydrocarbon chains of the same isotope [61]. While the δCH_2 mode of the less dense hexagonal packing is characterized by a singlet positioned at ~ 1467 cm^{-1} in the spectrum. The δCH_2 modes of the various models at 10 °C

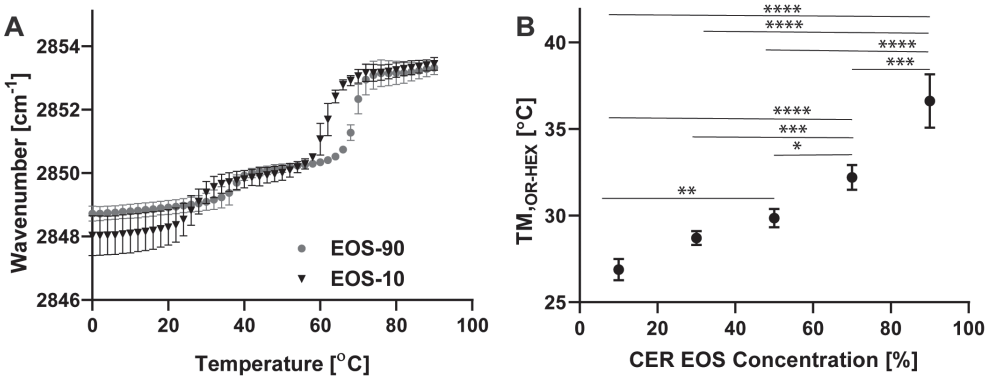

Fig. 3: The thermotropic response of the $\nu_s CH_2$ modes and midpoint temperatures of the orthorhombic-hexagonal phase transition ($T_{M,OR-HEX}$).

A) The initial wavenumber is higher in the EOS-90 than EOS-10 suggesting lower conformational ordering of the lipid chains in EOS-10. B) The $T_{M,OR-HEX}$ increases with CER EOS concentration. Differences between EOS 10 and 30, and between EOS 30 and 50 were not significant, while differences between EOS 10 and 50, EOS 10 and 70, EOS 10 and 90, EOS 30 and 70, EOS 30 and 90, EOS 50 and 70, EOS 50 and 90, and EOS 70 and 90 were significant. n ≥ 3, [*P < 0.05, **P < 0.01, ***P < 0.001, ****P < 0.0001].

and 32 °C are presented in Fig. 4A and B respectively. At 10 °C, the δCH_2 modes of all protiated models displayed two strong peaks typical of orthorhombic packing. At 32 °C, the δCH_2 modes in the spectrum of EOS-10, EOS-30, and EOS-50 exhibited strong central asymmetric peaks positioned at ~ 1467 cm^{-1} indicating an increased fraction of lipids adopting a hexagonal lateral packing at the expense of the fraction of lipids forming an orthorhombic packing (Fig. 4B). In contrast, EOS-70 and EOS-90 δCH_2 modes retained the two characteristic peaks attributed to orthorhombic packing.

The proportion of the liquid phase increases with CER EOS concentration

In a lipid mixture, selective deuteration of the various components enables the simultaneous monitoring of the conformational ordering and phase behavior of individual species [56]. This is because the vibrational energy of protiated and deuterated chains is sufficiently different when detected in the infrared spectrum. We deuterated the FFA chains in the various models. The compositions of the resulting samples are shown in table 1. The $\nu_s CD_2$ and $\nu_s CH_2$ peak positions attributed to DFFA and CER chains respectively were analyzed in the temperature range between 0 to 90 °C (Fig. 5A). At the initial temperature, $\nu_s CD_2$ peak positions were consistent with previous reports of high conformational ordering of the

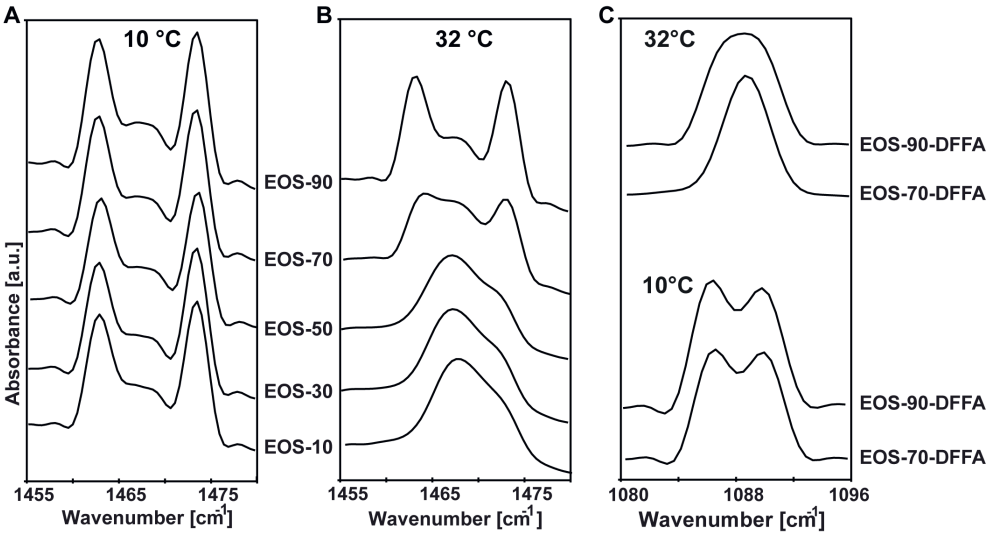

Fig. 4: δCH_2 and δCD_2 modes of the fully protiated and deuterated lipid models.

A) The δCH_2 frequencies at 10 °C display two distinct bands at approximately 1462 cm^{-1} and 1473 cm^{-1} indicating an orthorhombic lateral packing. B) At 32 °C (physiological temperature), EOS-10, 30, and 50 display a strong central peak indicating that a significant proportion of the lipids adopt the hexagonal phase. C) At 10 °C, EOS-70-DFFA and EOS-90 DFFA δCD_2 mode display weak splitting compared with the strong splitting of the δCD_2 mode of DFFA mixture [46] and transformed into single peaks at 32 °C, indicating that the FFAs are not phase separated.

methylene chains [46] indicating that the DFFA chains were highly crystalline, even at high CER EOS level. The $\nu_s CH_2$ mode of EOS-10-DFFA and EOS-30-DFFA revealed rearrangement of the protiated chain just before the hexagonal-liquid phase transition (between 60 and 80 °C), attributed to a high concentration of CER NS, as reported previously [46]. As the continued presence of orthorhombic packing in EOS-70 and EOS-90 at 32 °C in the fully protiated mixtures (Fig. 4B) could result from phase-separated FFA, we analyzed the δCH_2 and δDH_2 modes of the CER EOS/CER NS/CHOL/DFFAs mixtures. When deuterated and protiated chains are mixed in an orthorhombic lattice, the short-range coupling and peak splitting described in section 3.4 are eliminated as adjacent δCH_2 and δDH_2 modes will not interact due to differences in vibrational energy. Analysis of the CD_2 modes of EOS-70-DFFA and EOS-90-DFFA at 10 °C (Fig. 4C) showed significantly reduced peak splitting width compared with the maximum peak splitting in a fully deuterated environment that has been previously determined [46], indicating extensive mixing of the CERs and DFFA chains. At 32 °C, the CD_2 modes of EOS-70-DFFA and EOS-90-DFFA transformed to single peaks. This indicates that the orthorhombic packing at elevated temperatures cannot be due to phase-separated FFA.

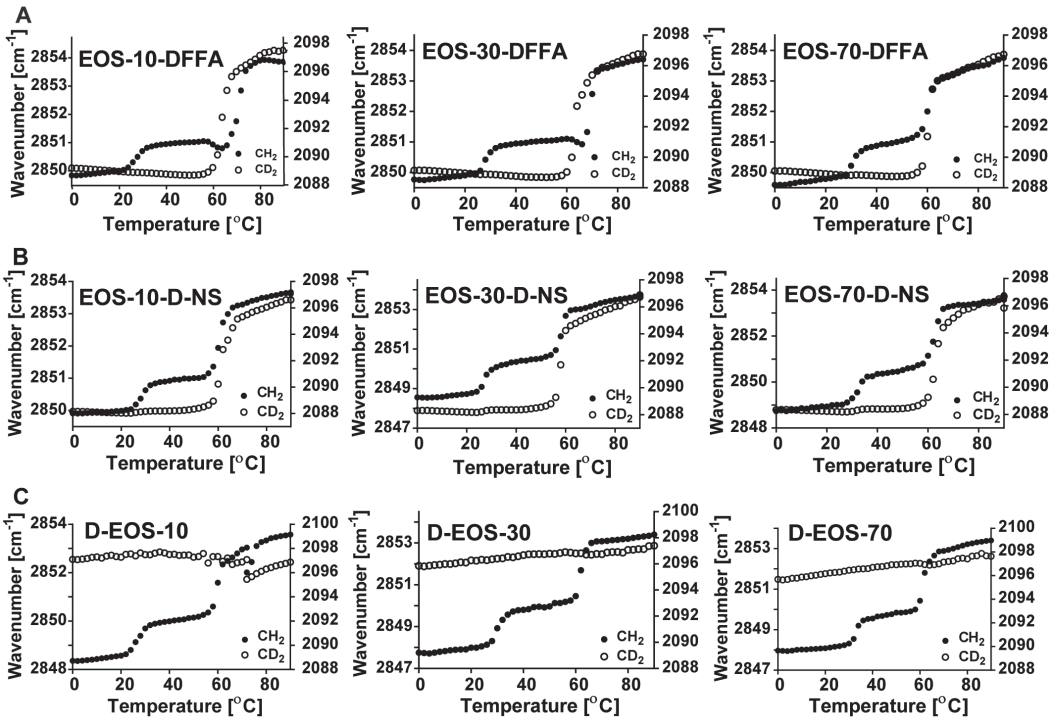

Fig. 5: Thermotropic response of the $\nu_s CH_2$ and $\nu_s CD_2$ modes of the partially deuterated lipid models.

The CH_2 (filled circle) and the CD_2 (open circle) peak positions are plotted on the primary y-axis and secondary y-axis respectively. The phase transition temperatures of the protiated and deuterated chains in the lipid models are displayed. A) FFA chains were deuterated. B) CER NS with deuterated C24 acyl chain. C) Deuterated oleate chain of CER EOS.

Lipid mixtures including CER NS with a deuterated C24 acyl chain were also examined. The $\nu_s CD_2$ modes of EOS-10 D-NS, EOS-30 D-NS, and EOS-70 D-NS were located initially at ~ 2088 cm^{-1} (Fig. 5B) indicating that CER NS chains are highly conformationally ordered in the lipid models, even at high CER EOS concentration. As the temperature increased, the order-disorder transition of the protiated chains and the deuterated CER NS chains occurred in the same temperature range. Finally, we analyzed the spectra of the lipid mixtures in which the linoleate moiety of CER EOS was replaced by deuterated oleate. The thermotropic response of the $\nu_s CH_2$ and $\nu_s CD_2$ modes of D-EOS-10, D-EOS-30, and D-EOS70 are displayed in Fig. 5C.

In the models with deuterated oleate chains, the $\nu_s CD_2$ mode was located at a higher wavenumber, ~ 2097 cm^{-1} from 0 until 90 °C, indicating that the oleate chains were disordered across the temperature range. Analysis of the $\nu_s CD_2$ peak

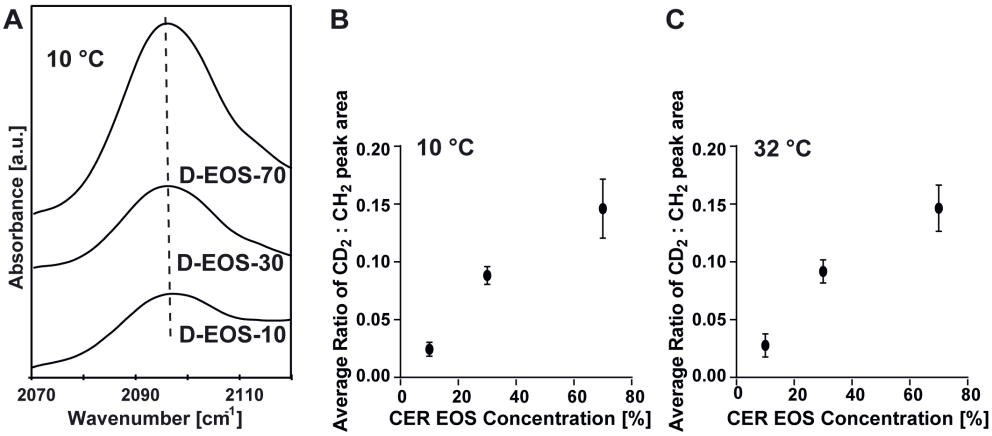

Fig. 6: Peak position of $\nu_s CD_2$, peak area ratio of $\nu_s CD_2$ to $\nu_s CD_2$, and correlation to permeability.

A) Mixtures with deuterated oleate chains of CER EOS show no shift in peak positions with increasing CER EOS concentration. B) and C) The average ratio of CD_2 (attributed to the disordered oleate) to CH_2 symmetric stretching peak area at 10 and 32 °C indicates an increase in the proportion of lipid fraction in the liquid phase with CER EOS concentration.

position at 10 °C revealed no shift in peak positions with increasing CER EOS-O concentration (Fig. 6A).

To evaluate the proportion of the liquid phase in the models, we compared the ratio of $\nu_s CD_2$ peak area (disordered) to $\nu_s CH_2$ peak area (crystalline) in the mixtures with deuterated oleate chains at 10 and 32 °C (Fig. 6B and C). There was a gradual increase in the ratio of the liquid/crystalline symmetric stretching peak area with increasing CER EOS-O content.

CER EOS concentration affects the LPP repeat distance

The influence of CER EOS concentration on the lamellar phase behavior of SC lipid models was studied. The SAXD profiles of the models with a gradual increase in CER EOS content are displayed in Fig. 7A-E. In CER EOS-10, the lipids form both the SPP and LPP with repeat distances of 5.4 and 12.2 nm respectively. Increasing the concentration of CER EOS from 10 to 30% resulted in the disappearance of the SPP. No significant difference in LPP repeat distance was observed between EOS-10 and EOS-30. Further increase in CER EOS concentration to 50, 70, and 90%, resulted in a gradual increase in LPP repeat distance (Fig. 7F) and the intensity ratio between the 2nd and 1st order of the LPP decreased concurrently. The diffraction curve of CER EOS-90, showed the 6th order to be absent, while the 1st order intensity surpassed the 2nd order, thus deviating from the characteristic

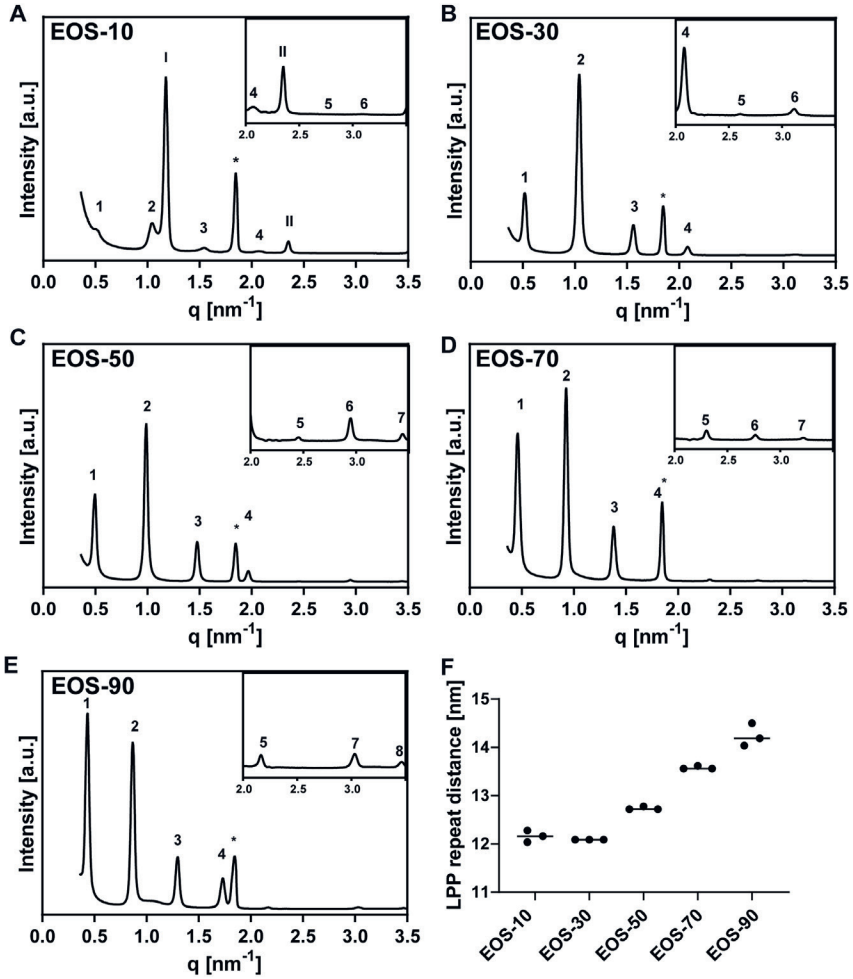

Fig. 7: X-ray diffraction profile of the lipid models.

The arabic numbers 1-8 indicate the diffraction orders of the LPP, while the roman numbers I and II indicate the diffraction orders of the SPP. A) In the diffraction profile of EOS-10, a series of diffraction peaks positioned at q = 0.52, 1.04, 1.52, 2.09, 2.53, and 3.03 nm^{-1} indicate the 1st, 2nd, 3rd, 4th, 5th, and 6th diffraction orders attributed to the LPP with a repeat distance of 12.2 nm and peaks positioned at q = 1.17 and 2.34 nm^{-1} indicate the 1st and 2nd diffraction orders attributed to the SPP with a repeat distance of 5.4 nm. B) In the diffraction profile of EOS-30, the peak positions at q = 0.52, 1.03, 1.56, 2.07, 2.60, and 3.11 nm^{-1} indicate the 1st -6th diffraction orders attributed to the LPP with a repeat distance of 12.2 nm. C) In the diffraction pattern of EOS-50, the peak positions at q = 0.49, 0.99, 1.48, 1.97, 2.46, 2.95, and 3.45 nm^{-1} are attributed to 1st-7th diffraction orders of the LPP with a repeat distance of 12.7 nm. D) In the diffraction pattern of EOS-70, the reflections at q = 0.46, 0.92, 1.38, 1.84 (overlapping the CHOL peak), 2.3, 2.76, and 3.22 nm^{-1} are attributed to the 1st-7th diffraction orders of the LPP with a repeat distance of 13.6 nm. E) In the diffraction pattern of EOS-90, the peak positions at q = 0.43, 0.87, 1.31, 1.73, 2.16, 3.02, and 3.46 nm^{-1} are attributed to 1st, 2nd, 3rd, 4th, 5th, 7th, and 8th diffraction orders of the LPP with a repeat distance of 14.4 nm. The 6th order peak was absent, The reflections at q = 1.85 nm^{-1} indicated by * in all the models are attributed to phase-separated CHOL. F) Graph showing an increase of LPP repeat distance with CER EOS concentration.

LPP intensity distribution (2nd order peak taller than 1st and 3rd order peaks), which has been described previously [46, 62].

DISCUSSION

For the first time, the influence of a gradual increase of CER EOS over a wide range of concentrations, namely from 10 % to 90% of the CER fraction of SC models was investigated. Despite the crucial role of CER EOS in the LPP formation, its influence on lipid phase behavior and barrier function are not entirely comprehended. To understand the skin barrier thoroughly, knowledge of the molecular arrangement of the lamellar unit cell is vital [12]. Previous experiments have identified that the linoleate chain of CER EOS is located in the inner head group regions and in the central region of the trilayer LPP, while the C(30) acyl chain extends from the boarders of the unit cell towards the central layer [12, 63]. It has been suggested that the linoleate/oleate moiety in the matrix could be a key element contributing to the SC impermeability by acting as an obstacle for the diffusion of hydrophilic compounds through the SC and traps for the apolar species [42]. The results from the current study have shown that this hypothesis does not hold when CER EOS concentration is ≥70%.

The SC lipid matrix is endowed with a characteristic composition and organization required for the barrier function. The physiological concentration of CER EOS in the SC is associated with low permeability indicating good barrier function. Data from our study shows that the barrier capability of the SC model is maintained somewhat up to a 50% increase in CER EOS concentration. Such robustness is an advantage to withstand the numerous challenges faced by the body due to the external environment.

Effect of CER EOS concentration on barrier function

In SC lipid model systems, CER EOS induces a co-existence of crystalline and disordered liquid domains. We examined the impact of increasing CER EOS concentration on the permeability of the SC lipid models. The results show that the permeability of the membrane to E-PABA did not differ when CER EOS concentration was raised from 10 to 30% of the total CER content. Similarly, it was reported that the permeability of indomethacin and theophylline through a complex lipid model was not improved when the concentration of either individual acylCER or an acylCER mixture was raised above the physiological concentration to 30% [43]. In contrast, a previous study demonstrated that the

permeability of a SC model prepared with pig CERs with CER EOS concentration of 14% was reduced when an additional 20% mol CER EOS was incorporated [64]. However, in this case, the difference is not solely due to the difference in the acylCER content as isolated pig CERs were used, which contain a wide distribution in chain lengths, while the additional synthetic CER EOS had only a single-chain length. Thus a change in chain length distribution might also have affected the permeability as demonstrated previously [64]. Opalka et al. also reported a reduction in the permeability of a simple SC model membrane when the concentration of CER EOS was increased from 10 to 30% [31]. In their study, there was also a reduction in the LPP repeat distance when increasing the CER EOS content from 10 to 30%, while we observed no difference. The LPP peak intensity distribution in their study also differed from ours, signifying a different structure.

In the present study, E-PABA steady-state flux only increased when CER EOS concentration was raised to 50%, becoming significantly higher when raised to ≥70%. This finding was corroborated by the TEWL values, which were also significantly higher for EOS-70 and EOS-90.

Effect of CER EOS concentration on lateral lipid organization

Several studies have associated a higher lipid chain packing density with reduced permeability of SC model membranes [32, 64, 65]. This relationship was not observed in the current study. The remarkably high permeability of EOS-70 and EOS-90 was irrespective of the presence of a high concentration of lipids forming an orthorhombic phase at 32 °C, the physiological temperature at which the permeation studies were carried out. Analysis of the FTIR data showed that the increased permeability was not due to phase separation as the hexagonal-liquid phase transition of FFA and CERs occurred in the same temperature range and the scissoring vibrations demonstrated mixing of the CERs and FFA chains in the EOS-70 and EOS-90 models. Thus, the delayed orthorhombic-hexagonal phase transition observed in the δCD_2 modes of EOS-70 and EOS-90 may be attributed to the increased level of the exceptionally long acyl chain of CER EOS.

To study the behavior of the unsaturated C18 acyl chain moiety of CER EOS, we used mixtures in which the oleate moiety of CER EOS-O was deuterated (Table 1). Several studies have reported a similar phase behavior for CER EOS-L and CER EOS-O containing mixtures. de Sousa et al. [48] analyzed equimolar mixtures of CERs, CHOL, and FFAs. The CER fraction contained either 30 mol% CER EOS-L or 30 mol% CER EOS-O. The results showed that the model prepared

with CER EOS-L and that prepared with the oleate analogue have a similar lipid phase behavior, both resulting in similar phase transition temperatures and leading to exclusive formation of the LPP with similar repeat distance. Bouwstra et al. [37] reported similar phase behavior in model mixtures with human CERs containing either synthetic CER EOS-L or synthetic CER EOS-O. In both mixtures, the LPP, as well as the SPP with very similar repeat distances, were formed. In addition using CER EOS-L, with the linoleate chain deuterated, Janssens et al. [41] determined that the linoleate moiety of CER EOS-L was already disordered at 20 °C indicated by the high δCD_2 wavenumber of 2099 cm^{-1}, which were very similar values as that of the deuterated oleate chain of CER EOS in this present study. Based on these studies we conclude that CER EOS linoleate and CER EOS oleate are very similar as far as the conformational ordering and the phase behavior is concerned, which are the properties we focused on in the present study.

In the spectrum of CER D-EOS-O/CER NS/CHOL/FFAs mixtures, the deuterated oleate chains were in the liquid phase in the entire temperature range studied (0-100°C). Despite increasing CER EOS concentration, there was no increasing shift in the $\nu_s CD_2$ frequencies of the deuterated oleate chains to indicate any further degree of disordering. In mixtures with the deuterated oleate the CD_2:CH_2 peak area ratio is an indication of the proportion of the liquid phase; an increase in this ratio with CER EOS concentration is observed.

Based on the carbon number in the model mixtures, the total fraction of CER moiety that is liquid in EOS-10 is 2.7% of the total CER volume and 1% of the total lipid volume given the equimolar ratio of CERs, FFAs, and CHOL. Likewise, the liquid fraction of the total lipids in EOS-30 and EOS-70 are 2.7% and 6.4% respectively. At very high CER EOS concentration (≥70%), the disordered linoleate located in the inner head group regions and the central layer of the LPP probably can no longer act as isolated fluid droplets that trap materials. Rather, there is a sufficient fraction of the disordered phase to increase the transport of substances along the inner headgroup region through the SC model membrane. Thus, the increased permeability of the SC models when CER EOS concentration is increased may be attributed to the increased proportion of the liquid phase. Our data demonstrate that the contribution of the increased fraction of lipids forming a disordered phase impacted more the barrier than the higher fraction of lipids forming the orthorhombic phase.

Effect of CER EOS concentration on lamellar organization

To gain insight into the relationship between SC lipid composition and lipid organization, SC model systems based on either isolated CERs or synthetic CERs are used [32, 50, 62, 66]. The SAXD peaks' position and their intensity can provide information about the lamellar structure within a sample [67]. In the present study, a two CER subclass model, EOS-10, which contained near physiological acylCER concentration formed both the SPP and LPP, mimicking the lamellar organization found in the extracellular lipid of native human SC. A previous study also reported the presence of the SPP and LPP in a simple five-component SC model (CER EOS/CER NS/CHOL/FFA(C24)/CHOL sulphate) with CER EOS also constituting 10% of the CER content [31]. In that same study, a more complex SC model (with a higher number of CERs and FFAs subclasses) also containing 10% CER EOS did not exhibit the formation of the LPP. Only when a mixture of acylCERs with different sphingoid bases was incorporated in the complex model could both the SPP and LPP be formed. In contrast, other complex SC models mimicking porcine [50, 62, 66] or human SC [32] CER composition incorporating a single acylCER subclass (15% CER EOS) or even 7% CER EOS in diseased skin model [32], resulted in the formation of both the SPP and LPP. The difference in the lipid organization obtained for SC models containing single acylCER may be due to the differences in the preparation method as previously reported [46]. The model prepared with an acylCER mixture may be less sensitive to such differences in the preparation method as seen by its formation of both the SPP and LPP.

When we increased CER EOS concentration from 10 to 30%, only the LPP was present. Exclusive formation of the LPP has been associated with a high content of CER EOS in SC models containing 30-40% CER EOS in their CER fraction [31, 44, 45, 62, 68]. The LPP diffraction peaks of EOS-10 and EOS-30 exhibited the intensity distribution corresponding to that in the unit cell of a complex SC model and the native SC LPP (2^{nd} order peak more intense than 1^{st} and 3^{rd} order peaks) as described previously [46, 62] indicating similarity in the basic LPP structure. This finding supports the use of simple models with fewer components for a more detailed evaluation of the effect of individual lipid components on the lipid organization of SC models. Simple SC models modified in composition to form exclusively the LPP have been employed for a detailed study of the LPP structure, lipid arrangement, and molecular interaction within the LPP [12, 42, 45, 46, 68]. However, when CER EOS concentration was raised to 90 mol% the LPP intensity distribution deviated. The 1^{st} order LPP peak became more intense than the 2^{nd}. Together with the very long repeat distance (14.4 nm), this demonstrates that the lipids form a different molecular organization than the typical SC's LPP structure.

CONCLUSIONS

In the present paper, we have advanced the previously reported studies of disordered lipid domains in the crystalline SC model, attributed to the unsaturated fatty acid moiety of CER EOS. Increasing CER EOS concentration induced a higher fraction of lipids forming orthorhombic and liquid phases at the expense of the hexagonal phase. Only when CER EOS concentration was raised to ≥ 70%, did the permeability of the SC model increase significantly. This could be attributed to the increased fraction of lipids forming a liquid phase. Such sturdiness contributes to the skin's primary function which is to protect the body from the invasion of pathogens and other harmful substances in the external environment as well as preventing uncontrolled loss of fluid from the body.

ACKNOWLEDGEMENTS

We thank the company Evonik for the donation of several CER subclasses. We also acknowledge the staff at the DUBBLE beamline 26B at the ESRF, Grenoble, France for assisting with the X-ray diffraction measurements.

REFERENCES

1. Elias, P. M., Stratum corneum defensive functions: an integrated view. *J. Invest. Dermatol.* **2005,** *125* (2), 183-200.
2. Baroni, A.; Buommino, E.; De Gregorio, V.; Ruocco, E.; Ruocco, V.; Wolf, R., Structure, and function of the epidermis related to barrier properties. *Clin. Dermatol.* **2012,** *30* (3), 257-62.
3. Madison, K. C., Barrier function of the skin: "la raison d'etre" of the epidermis. *J. Invest. Dermatol.* **2003,** *121* (2), 231-41.
4. Bodde, H. E.; Kruithof, M. A. M.; Brussee, J.; Koerten, H. K., Visualization of normal and enhanced Hgcl2 transport through human-skin invitro. *Int. J. Pharm.* **1989,** *53* (1), 13-24.
5. Talreja, P. S.; Kleene, N. K.; Pickens, W. L.; Wang, T. F.; Kasting, G. B., Visualization of the lipid barrier and measurement of lipid pathlength in human stratum corneum. *AAPS Pharmsci.* **2001,** *3* (2), art. no. 13.
6. Proksch, E.; Brandner, J. M.; Jensen, J. M., The skin: an indispensable barrier. *Exp. Dermatol.* **2008,** *17* (12), 1063-72.
7. Wickert, R. R.; Visscher, M. O., Structure and function of the epidermal barrier. *Am J Infect Control* **2006,** *34* (10), S98-S110.
8. Bouwstra, J. A.; Gooris, G. S.; van der Spek, J. A.; Bras, W., Structural investigations of human stratum corneum by small-angle X-ray scattering. *J. Invest. Dermatol.* **1991,** *97* (6), 1005-12.
9. White, S. H.; Mirejovsky, D.; King, G. I., Structure of lamellar lipid domains and corneocyte envelopes of murine stratum corneum. An X-ray diffraction study. *Biochemistry* **1988,** *27* (10), 3725-32.
10. de Jager, M.; Groenink, W.; Bielsa i Guivernau, R.; Andersson, E.; Angelova, N.; Ponec, M.; Bouwstra, J., A novel in vitro percutaneous penetration model: evaluation of barrier properties with p-aminobenzoic acid and two of its derivatives. *Pharm. Res.* **2006,** *23* (5), 951-60.
11. Groen, D.; Poole, D. S.; Gooris, G. S.; Bouwstra, J. A., Is an orthorhombic lateral packing and a proper lamellar organization important for the skin barrier function? *Biochim. Biophys. Acta* **2011,** *1808* (6), 1529-1537.
12. Mojumdar, E. H.; Gooris, G. S.; Groen, D.; Barlow, D. J.; Lawrence, M. J.; Deme, B.; Bouwstra, J. A., Stratum corneum lipid matrix: Location of acyl ceramide and cholesterol in the unit cell of the long periodicity phase. *Biochim. Biophys. Acta* **2016,** *1858* (8), 1926-34.
13. Madison, K. C.; Swartzendruber, D. C.; Wertz, P. W.; Downing, D. T., Presence of intact intercellular lipid lamellae in the upper layers of the stratum corneum. *J. Invest. Dermatol.* **1987,** *88* (6), 714-8.
14. Damien, F.; Boncheva, M., The extent of orthorhombic lipid phases in the stratum corneum determines the barrier efficiency of human skin in vivo. *J. Invest. Dermatol.* **2010,** *130* (2), 611-614.
15. Weerheim, A.; Ponec, M., Determination of stratum corneum lipid profile by tape stripping in combination with high-performance thin-layer chromatography. *Arch. Dermatol. Res.* **2001,** *293* (4), 191-199.
16. Coderch, L.; López, O.; de la Maza, A.; Parra, J. L., Ceramides and Skin Function. *Am. J. Clin. Dermatol.* **2003,** *4* (2), 107-129.
17. Wertz, P.W.; Dowing, D.T., *Physiology, biochemistry and molecular biology of the skin*. second ed.; Oxford University Press: New York, 1991; Vol. 1, p 205-236.

18. Norlen, L.; Nicander, I.; Lundsjo, A.; Cronholm, T.; Forslind, B., A new HPLC-based method for the quantitative analysis of inner stratum corneum lipids with special reference to the free fatty acid fraction. *Arch. Dermatol. Res.* **1998,** *290* (9), 508-16.

19. Masukawa, Y.; Narita, H.; Shimizu, E.; Kondo, N.; Sugai, Y.; Oba, T.; Homma, R.; Ishikawa, J.; Takagi, Y.; Kitahara, T.; Takema, Y.; Kita, K., Characterization of overall ceramide species in human Stratum corneum. *J. Lipid Res.* **2008,** *49* (7), 1466-1476.

20. Rabionet, M.; Gorgas, K.; Sandhoff, R., Ceramide synthesis in the epidermis. *Biochim. Biophys. Acta* **2014,** *1841* (3), 422-34.

21. Robson, K. J.; Stewart, M. E.; Michelsen, S.; Lazo, N. D.; Downing, D. T., 6-Hydroxy-4-sphingenine in human epidermal ceramides. *J. Lipid Res.* **1994,** *35* (11), 2060-8.

22. Stewart, M. E.; Downing, D. T., A new 6-hydroxy-4-sphingenine-containing ceramide in human skin. *J. Lipid Res.* **1999,** *40* (8), 1434-9.

23. van Smeden, J.; Hoppel, L.; van der Heijden, R.; Hankemeier, T.; Vreeken, R. J.; Bouwstra, J. A., LC/MS analysis of stratum corneum lipids: ceramide profiling and discovery. *J. Lipid Res.* **2011,** *52* (6), 1211-21.

24. Janssens, M.; van Smeden, J.; Gooris, G. S.; Bras, W.; Portale, G.; Caspers, P. J.; Vreeken, R. J.; Kezic, S.; Lavrijsen, A. P.; Bouwstra, J. A., Lamellar lipid organization and ceramide composition in the stratum corneum of patients with atopic eczema. *J. Invest. Dermatol.* **2011,** *131* (10), 2136-8.

25. van Smeden, J.; Janssens, M.; Boiten, W. A.; van Drongelen, V.; Furio, L.; Vreeken, R. J.; Hovnanian, A.; Bouwstra, J. A., Intercellular skin barrier lipid composition, and organization in Netherton syndrome patients. *J. Invest. Dermatol.* **2014,** *134* (5), 1238-1245.

26. Schreiner, V.; Gooris, G. S.; Pfeiffer, S.; Lanzendorfer, G.; Wenck, H.; Diembeck, W.; Proksch, E.; Bouwstra, J., Barrier characteristics of different human skin types investigated with X-ray diffraction, lipid analysis, and electron microscopy imaging. *J. Invest. Dermatol.* **2000,** *114* (4), 654-60.

27. J.A. Bouwstra, E. H. M., *Cosmetic formulation principles and practice*. CRC Press: Boca Raton, 2019.

28. Crumrine, D.; Khnykin, D.; Krieg, P.; Man, M.-Q.; Celli, A.; Mauro, T. M.; Wakefield, J. S.; Menon, G.; Mauldin, E.; Miner, J. H.; Lin, M.-H.; Brash, A. R.; Sprecher, E.; Radner, F. P. W.; Choate, K.; Roop, D.; Uchida, Y.; Gruber, R.; Schmuth, M.; Elias, P. M., Mutations in Recessive Congenital Ichthyoses Illuminate the Origin and Functions of the Corneocyte Lipid Envelope. *J. Investig. Dermatol.* **2019,** *139* (4), 760-768.

29. Eckl, K.-M.; Tidhar, R.; Thiele, H.; Oji, V.; Hausser, I.; Brodesser, S.; Preil, M.-L.; Önal-Akan, A.; Stock, F.; Müller, D.; Becker, K.; Casper, R.; Nürnberg, G.; Altmüller, J.; Nürnberg, P.; Traupe, H.; Futerman, A. H.; Hennies, H. C., Impaired Epidermal Ceramide Synthesis Causes Autosomal Recessive Congenital Ichthyosis and Reveals the Importance of Ceramide Acyl Chain Length. *J. Investig. Dermatol.* **2013,** *133* (9), 2202-2211.

30. Motta, S.; Monti, M.; Sesana, S.; Caputo, R.; Carelli, S.; Ghidoni, R., Ceramide composition of the psoriatic scale. *Biochim. Biophys. Acta* **1993,** *1182* (2), 147-51.

31. Opalka, L.; Kovacik, A.; Maixner, J.; Vavrova, K., Omega-O-Acylceramides in skin lipid membranes: effects of concentration, sphingoid base, and model complexity on microstructure and permeability. *Langmuir* **2016,** *32* (48), 12894-12904.

32. Uche, L. E.; Gooris, G. S.; Bouwstra, J. A.; Beddoes, C. M., Barrier Capability of Skin Lipid Models: Effect of Ceramides and Free Fatty Acid Composition. *Langmuir* **2019,** *35* (47), 15376-15388.

33. t'Kindt, R.; Jorge, L.; Dumont, E.; Couturon, P.; David, F.; Sandra, P.; Sandra, K., Profiling and characterizing skin ceramides using reversed-phase liquid chromatography–quadrupole time-of-flight mass spectrometry. *Anal. Chem.* **2012,** *84* (1), 403-411.

34. van Smeden, J.; Bouwstra, J. A., Stratum corneum lipids: Their role for the skin barrier function in healthy subjects and atopic dermatitis patients. *Curr. Probl. Dermatol.* **2016,** *49*, 8-26.

35. McIntosh, T. J.; Stewart, M. E.; Downing, D. T., X-ray diffraction analysis of isolated skin lipids: reconstitution of intercellular lipid domains. *Biochemistry* **1996,** *35* (12), 3649-53.

36. Bouwstra, J. A.; Gooris, G. S.; Dubbelaar, F. E.; Ponec, M., Phase behavior of lipid mixtures based on human ceramides: coexistence of crystalline and liquid phases. *J. Lipid Res.* **2001,** *42* (11), 1759-70.

37. Bouwstra, J. A.; Gooris, G. S.; Dubbelaar, F. E.; Ponec, M., Phase behavior of stratum corneum lipid mixtures based on human ceramides: the role of natural and synthetic ceramide 1. *J. Invest. Dermatol.* **2002,** *118* (4), 606-17.

38. Bouwstra, J. A.; Gooris, G. S.; Dubbelaar, F. E.; Weerheim, A. M.; Ijzerman, A. P.; Ponec, M., Role of ceramide 1 in the molecular organization of the stratum corneum lipids. *J. Lipid Res.* **1998,** *39* (1), 186-96.

39. de Jager, M. W.; Gooris, G. S.; Ponec, M.; Bouwstra, J. A., Lipid mixtures prepared with well-defined synthetic ceramides closely mimic the unique stratum corneum lipid phase behavior. *J. Lipid Res.* **2005,** *46* (12), 2649-2656.

40. Pham, Q. D.; Mojumdar, E. H.; Gooris, G. S.; Bouwstra, J. A.; Sparr, E.; Topgaard, D., Solid and fluid segments within the same molecule of stratum corneum ceramide lipid. *Quarterly Reviews of Biophysics* **2018,** *51*.

41. Janssens, M.; Gooris, G. S.; Bouwstra, J. A., Infrared spectroscopy studies of mixtures prepared with synthetic ceramides varying in head group architecture: coexistence of liquid and crystalline phases. *Biochim. Biophys. Acta* **2009,** *1788* (3), 732-742.

42. Paz Ramos, A.; Gooris, G.; Bouwstra, J.; Lafleur, M., Evidence of hydrocarbon nanodrops in highly ordered stratum corneum model membranes. *J. Lipid Res.* **2018,** *59* (1), 137-143.

43. Opalka, L.; Kovacik, A.; Pullmannova, P.; Maixner, J.; Vavrova, K., Effects of omega-O-acylceramide structures and concentrations in healthy and diseased skin barrier lipid membrane models. *J. Lipid Res.* **2020,** *61* (2), 219-228.

44. Gooris, G. S.; Kamran, M.; Kros, A.; Moore, D. J.; Bouwstra, J. A., Interactions of dipalmitoylphosphatidylcholine with ceramide-based mixtures. *Biochim. Biophys. Acta* **2018,** *1860* (6), 1272-1281.

45. Beddoes, C. M.; Gooris, G. S.; Bouwstra, J. A., Preferential arrangement of lipids in the long-periodicity phase of a stratum corneum matrix model. *J. Lipid Res.* **2018,** *59* (12), 2329-2338.

46. Uche, L. E.; Gooris, G. S.; Beddoes, C. M.; Bouwstra, J. A., New insight into phase behavior and permeability of skin lipid models based on sphingosine and phytosphingosine ceramides. *Biochim. Biophys. Acta* **2019,** *1861* (7), 1317-1328.

47. Boiten, W.; Absalah, S.; Vreeken, R.; Bouwstra, J.; van Smeden, J., Quantitative analysis of ceramides using a novel lipidomics approach with three dimensional response modelling. *Biochim. Biophys. Acta* **2016,** *1861* (11), 1652-1661.

48. de Sousa Neto, D.; Gooris, G.; Bouwstra, J., Effect of the omega-acylceramides on the lipid organization of stratum corneum model membranes evaluated by X-ray diffraction and FTIR studies (Part I). *Chem. Phys. Lipids* **2011,** *164* (3), 184-95.

49. de Jager, M.; Groenink, W.; van der Spek, J.; Janmaat, C.; Gooris, G.; Ponec, M.; Bouwstra, J., Preparation and characterization of a stratum corneum substitute for in vitro percutaneous penetration studies. *Biochim. Biophys. Acta* **2006,** *1758* (5), 636-44.

50. Mojumdar, E. H.; Helder, R. W.; Gooris, G. S.; Bouwstra, J. A., Monounsaturated fatty acids reduce the barrier of stratum corneum lipid membranes by enhancing the formation of a hexagonal lateral packing. *Langmuir* **2014,** *30* (22), 6534-43.

51. International Conference on Harmonization (ICH) Q2 (R1), Validation of analytical procedures: Text and Methodology. 2005.

52. European Pharmacopoeia. . 8 ed.; European Directorate for the quality of medicines & healthcare. Strasbourg, 2014; Vol. 1.

53. Oguri, M.; Gooris, G. S.; Bito, K.; Bouwstra, J. A., The effect of the chain length distribution of free fatty acids on the mixing properties of stratum corneum model membranes. *Biochim. Biophys. Acta* **2014,** *1838* (7), 1851-1861.

54. Wojdyr, M., Fityk: a general-purpose peak fitting program. *J Appl Crystallogr* **2010,** *43*, 1126-1128.

55. Snyder, R. G.; Liang, G. L.; Strauss, H. L.; Mendelsohn, R., IR spectroscopic study of the structure and phase behavior of long-chain diacylphosphatidylcholines in the gel state. *Biophys. J* . **1996,** *71* (6), 3186-98.

56. Mendelsohn, R.; Moore, D. J., Vibrational spectroscopic studies of lipid domains in biomembranes and model systems. *Chem. Phys. Lipids* **1998,** *96* (1-2), 141-57.

57. Mendelsohn, R.; Flach, C. R.; Moore, D. J., Determination of molecular conformation and permeation in skin via IR spectroscopy, microscopy, and imaging. *Biochim. Biophys. Acta* **2006,** *1758* (7), 923-933.

58. Mendelsohn, R.; Moore, D. J., Infrared determination of conformational order and phase behavior in ceramides and stratum corneum models. *Methods Enzymol.* **2000,** *312*, 228-47.

59. Gooris, G. S.; Bouwstra, J. A., Infrared spectroscopic study of stratum corneum model membranes prepared from human ceramides, cholesterol, and fatty acids. *Biophys. J.* **2007,** *92* (8), 2785-95.

60. Mendelsohn, R.; Liang, G. L.; Strauss, H. L.; Snyder, R. G., IR spectroscopic determination of gel state miscibility in long-chain phosphatidylcholine mixtures. *Biophys. J.* **1995,** *69* (5), 1987-1998.

61. Moore, D. J.; Rerek, M. E., Insights into the molecular organization of lipids in the skin barrier from infrared spectroscopy studies of stratum corneum lipid models. *Acta Derm-Venereol.* **2000**, 16-22.

62. Groen, D.; Gooris, G. S.; Bouwstra, J. A., New insights into the stratum corneum lipid organization by X-ray diffraction analysis. *Biophys. J.* **2009,** *97* (8), 2242-2249.

63. Mojumdar, E. H.; Gooris, G. S.; Barlow, D. J.; Lawrence, M. J.; Deme, B.; Bouwstra, J. A., Skin lipids: localization of ceramide and fatty acid in the unit cell of the long periodicity phase. *Biophys. J* . **2015,** *108* (11), 2670-2679.

64. Mojumdar, E. H.; Kariman, Z.; van Kerckhove, L.; Gooris, G. S.; Bouwstra, J. A., The role of ceramide chain length distribution on the barrier properties of the skin lipid membranes. *Biochim Biophys Acta* **2014,** *1838* (10), 2473-2483.

65. Skolova, B.; Jandovska, K.; Pullmannova, P.; Tesar, O.; Roh, J.; Hrabalek, A.; Vavrova, K., The role of the trans double bond in skin barrier sphingolipids: permeability and infrared spectroscopic study of model ceramide and dihydroceramide membranes. *Langmuir* **2014,** *30* (19), 5527-35.

66. de Jager, M. W.; Gooris, G. S.; Dolbnya, I. P.; Bras, W.; Ponec, M.; Bouwstra, J. A., Novel lipid mixtures based on synthetic ceramides reproduce the unique stratum corneum lipid organization. *J. Lipid Res.* **2004,** *45* (5), 923-32.

67. Wess, T. J.; Drakopoulos, M.; Snigirev, A.; Wouters, J.; Paris, O.; Fratzl, P.; Collins, M.; Hiller, J.; Nielsen, K., The use of small-angle x-ray diffraction studies for the analysis of structural features in archaeological samples. *Archaeometry* **2001,** *43*, 117-129.

68. Pullmannova, P.; Ermakova, E.; Kovacik, A.; Opalka, L.; Maixner, J.; Zbytovska, J.; Kucerka, N.; Vavrova, K., Long and very long lamellar phases in model stratum corneum lipid membranes. *J. Lipid Res* **2019,** *60* (5), 963-971.